Fabrication and Characterization of Mesocarbon Anode for Sodium-Ion Batteries

Dewi Idamayanti[1,3] , Achmad Rochliadi[2], Bambang Sunendar Purwasasmita[1], Brian Yuliarto[1] , and Ahmad Nuruddin[1(✉)]

[1] Department of Engineering Physics, Faculty of Industrial Technology, Institut Teknologi Bandung, Jl. Ganesa 10, Bandung 40132, Indonesia
nuruddin@tf.itb.ac

[2] Department of Chemistry, Faculty of Mathematics and Natural Science, Institut Teknologi Bandung, Jl. Ganesa 10, Bandung 40132, Indonesia

[3] Advance Materials Engineering Study Program, Department of Foundry Engineering, Politeknik Manufaktur Bandung, Bandung 40135, Indonesia

Abstract. This study investigated the properties of mesocarbon anodes in the half-cell of sodium-ion batteries. The behavior of mesocarbon was examined using electrochemical methods. Cyclic voltammetry (CV) was applied with various scan rates to reveal the anodic-cathodic voltage and peak current. The CV profile allowed for predicting the energy storage mechanism of sodium ions in mesocarbon. The CV measurement of the half-cell Na | mesocarbon demonstrated the intercalation and de-intercalation of sodium ions in the graphene interlayer at 0.01 V and 0.12 V, respectively. Based on the Power law, the kinetics of sodium ion movement was controlled by the diffusion-dominant reaction. After 25 cycles, the electrochemical impedance spectroscopy (EIS) spectra exhibited increasing resistances in the solid-electrolyte interface (R_{SEI}) and charge transfer (Rct), ranging from 53.8 to 65.6 Ω and 42.6 to 229 Ω, respectively. Considering the charge/discharge rate capability in the first five cycles, the mesocarbon could deliver a specific capacity of discharge of 42 mAh/g at 0.1 C and retain 73% of its capacity after 25 cycles.

Keywords: Mesocarbon · Sodium-ion battery · Anode

1 Introduction

The increasing market demands on the availability of power sources have greatly motivated the rechargeable batteries development. Lithium-ion batteries (LIBs) have been showing the best performance as devices for an energy storage system for three decades because of their high capability to store energy for long life cycles [1]. However, Li as a primary precursor of cathode materials for LIBs is in limited abundance (0.01%) and non-uniformly distributed in the earth's outer layer [2, 3]. Moreover, Li's price has increased up to 150% compared to 2018 due to the high demand for EVs [4]. Therefore, efforts have been devoted to finding alternative rechargeable batteries.

Sodium-ion batteries (SIBs) are a promising candidate to complement LIBs because of their abundance level of sodium sources in the earth (2.83%), low cost, and relatively less safety concern [5, 6]. In addition, SIBs have similar physical and chemical properties to LIBs [7], having a sodium potential of -2.7 V approach to the lithium potential of -3.0 V. Similar to LIBs, a typical SIBs configuration is a cathode, anode, separator, and electrolyte. The performance of SIBs strongly depends on the electro-active materials properties for cathode and anode [1].

In the field of anode materials, SIBs has employed carbonaceous materials, transition metal oxides, and intermetallic and organic compound [5]. Graphite as a carbon-based materials are the anode choice for LIBs by condering their high gravimetric and volumetric capacity, and low cost. In the case of SIBs, sodium-ion faces a significant barrier for intercalation into graphite [8] due to the thin graphene interlayer distance. Due to the similarity mechanism with LIBs, SIBs can employ the active materials used in LIBs. Mesocarbon microbead is one of the carbonaceous materials recognized as a superior anode for LIBs [9]. The unique microstructure of mesocarbon offers the opportunity to be an anode for SIBs, as observed by Alcantara et al. [10]. In this report, we analyzed the electrochemical behavior of mesocarbon anode for SIBs using electrochemical measurements.

2 Experimental Section

2.1 Materials and Procedures

Mesocarbon powder was obtained from KGC, Ltd, Indonesia. Materials used from Sigma Aldrich were acetylene black, polyvinyl-pyrrolidone (PVDF), ethylene carbonate ($C_3H_4O_3$), dimethyl carbonate ($C_3H_6O_3$), and sodium perchlorate ($NaClO_4$). Sodium metals were obtained from Merck. All chemical reagents were used without further treatment. The mesocarbon anode was made by blending 85 wt.% mesocarbon and 5 wt.% acetylene black in 10 wt.% polyvinyl-pyrrolidone under mechanical stirring and the slurry was formed. Furthermore, the slurry was coated on an aluminum foil surface and then heated at 80 °C for 24 h. The mesocarbon-coated aluminum was punched into a 16 mm diameter coin shape and heat treated in a vacuum environment at 120 °C for 4 h.

2.2 Characterization

The observation of mesocarbon morphology was carried out using a SEM (scanning electron microscope, Hitachi SU3500) operated at 4 kV. The microstructure of mesocarbon was measured by X-ray diffractometer (XRD, D8 Advance), with Cu target (λ = 0.154056 nm).

2.3 Electrochemical Testing

The mesocarbon anode properties were measured in a quick assembly coin cell. The half-cell contained mesocarbon anode with a loading mass of 4 mg/cm^2 and a mixture

of NaClO$_4$ 1 M in C$_3$H$_4$O$_3$, and C$_3$H$_6$O$_3$ (1:1) as electrolyte. Separator used in this study was Whatman GF/C and sodium foil as a counter electrode and reference electrode. The coin cell assembling was carried out in an ultra-high purity N$_2$-filled glove box. CV measurement was performed at a scan rate of 0.1 mV/s for voltage 0.001–1.5 V. EIS measurement was carried out at frequency 1.5 MHz–1 Hz with an amplitude of 5 mV. The GCD was measured using potentiostat/galvanostat (Corrtest CS350). The half-cell was cycled in the voltage window from 0.001 V to 2.5 V at room temperature.

3   Results and Discussion

The SEM morphology of commercial mesocarbon is shown in Fig. 1a. As shown in the figure, such mesocarbon has nonhomogeneous shapes consisting of spherical and irregular particles. The XRD diffraction peak of mesocarbon (Fig. 1b) exhibits a very sharp and symmetric (002) peak at 26.3°, which corresponds to highly ordered graphite microcrystalline. The d-spacing value (d$_{002}$), which is associated with graphene interlayer distance within mesocarbon, is simulated by a profile-fitting process and then calculated using Bragg's law equation as follows:

$$d_{002} = \frac{\lambda}{2\sin\theta} \tag{1}$$

The mesocarbon possesses d$_{002}$ of 0.334 nm, which indicates the mesocarbon contains a dominantly graphitic structure, as previously reported by Yan and Wang [10].

Despite d$_{002}$ spacing being too small for interlayer insertion of sodium-ion [9], the CV curve shows that the intercalation/de-intercalation of sodium-ion may still occur in mesocarbon for the first three cycles, as depicted in Fig. 2. It indicates a stable and reversible reaction during the intercalation/de-intercalation. The sharp peak of cathodic at ~0.001 V and anodic at ~0.12 V is ascribed to sodium-ion intercalation and de-intercalation, respectively [11]. There is no solid electrolyte interface (SEI) formation at around 0.4 V, which means the electrolyte's decomposition does not occur or the cathodic current is not detected.
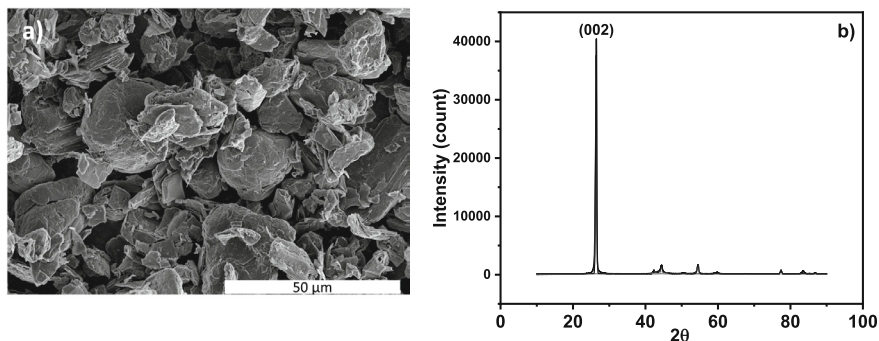
Fig. 1. SEM image (a) and XRD pattern (b) of mesocarbon.
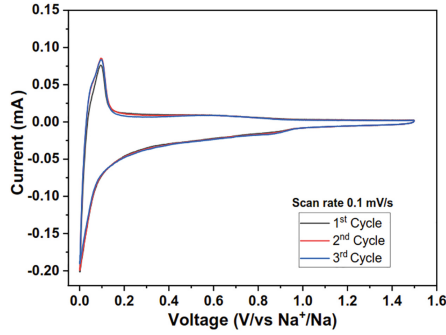
Fig. 2. Cyclic voltammogram of the first three cycles of mesocarbon anode.

At Fig. 3, the kinetic analysis of electrode material can be derived from the CV graph for five scan rates to study the energy storage mechanism and kinetic reaction. This characteristic feature can estimate the contribution of diffusion-controlled or surface-controlled currents to the total charge measured as proposed by Ardizzone et al. [12]. Diffusion-controlled current is attributed to intercalation/de-intercalation behavior, while surface-controlled current is related to capacitive characteristics. Therefore, the CV curve is represented by capacitive and diffusion currents. According to Power's law, the total charge (it) could be expressed through the following equation [14]:

$$i_t = i_{capacitive} + i_{diffusion} = a\upsilon^b \tag{2}$$

$$\log i_t = \log a + b. \log \upsilon \tag{3}$$

Equation (2) and (3) shows the relationship between the voltage-current response of electrodes at various scan rates where υ is the scan rate, and *a* and *b* values are adjustable. The *b*-value represents the slope of the line shown in Fig. 3b. If the *b*-value is 0.5, diffusion processes control the electrode kinetic. For the *b*-value is one, the electrode kinetic allows the surface-controlled methods associated with capacitive and
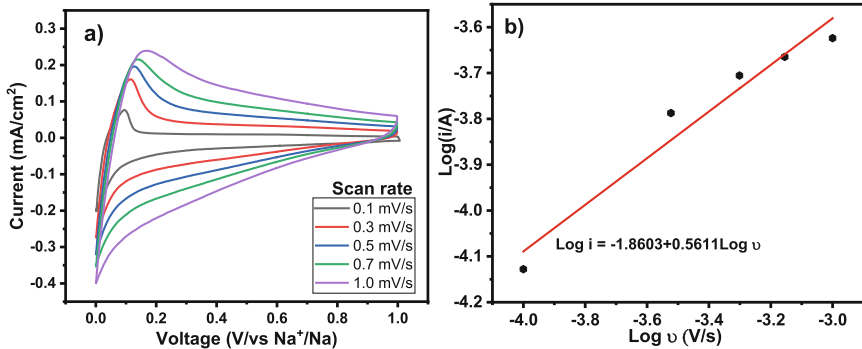

**Fig. 3.** Mesocarbon anode: (a) cyclic voltammogram, (b) the slope of Log i versus Log υ at different redox states.

pseudocapacitive behavior [13]. Figure 3a shows the CV curves for scan rates ranging from 0.1 to 1.0 mV/s. The anodic peaks at ~0.12 V are selected for kinetic analysis, and a plot of the log υ − log i have a linear relationship. The fitted b-value is 0.509, indicating that the kinetic is controlled by diffusion process.

EIS was generally used to distinguish the resistance before and after cycles. The intermediate-frequency semicircles correspond to the interface of the films' solid-electrolyte resistance (SEI). The second semicircles represent the charge transfer resistance. Even though SEI film is not observed in the CV curve, it can be detected in the Nyquist plot, as presented in Fig. 4a. The linear portion corresponds with Warburg, indicating diffusion process of the sodium ions in the electrode material. The resistance value was determined by fitting the experimental EIS graph with the proposed equivalent circuit model, as shown in Fig. 4b. The resulting R_1, R_2, R_3, CPE1, CPE2, and W are the ohmic resistance, the SEI resistance (R_{SEI}), the charge-transfer resistance (R_{ct}), double layer capacitance of SEI, double layer capacitance of anode, and the Warburg impedance, respectively.

After cycling, mesocarbon results in the R_{SEI} and R_{ct} increase from 53.8 to 65.6 Ω and 42.6 to 229 Ω, respectively. The slight increase in R_{SEI} results from the electrolyte decomposition, which is deposited on the mesocarbon surface. It is evidenced in Fig. 5b that the SEI film covers the whole mesocarbon surface. Before cycling (Fig. 5a), the mesocarbon surface appears rough and porous microstructure.
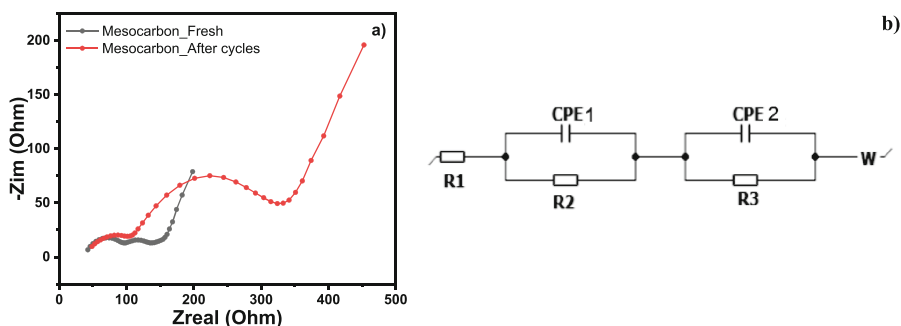
Fig. 4. Nyquist plot of the mesocarbon anode (a) and fitted Nyquist plot and circuit equivalent model (b), comparison in fresh and after cycles
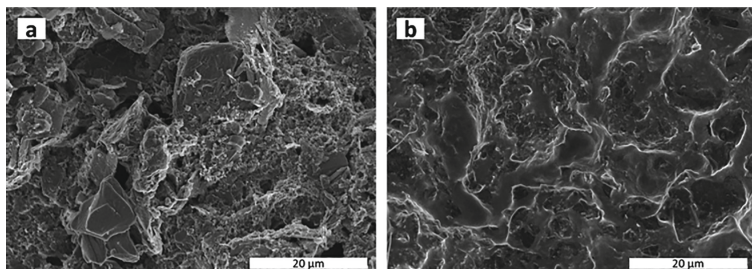
Fig. 5. SEM images of mesocarbon anode (a) before the cycle and (b) after cycles.
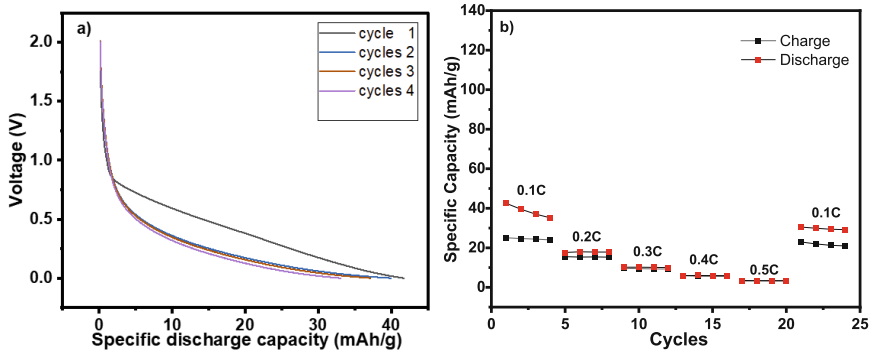
Fig. 6. Specific discharge capacity at 0.1 C (a) and rate-capability of the mesocarbon anode at different C-rate (b).

The SEI thickness mainly influences the increase of charge transfer resistance on the mesocarbon surface compared to the fresh mesocarbon. Furthermore, the formation of SEI leads to irreversible capacity owing to sodium-ion consumption [14], then reduces the capacity of discharge from 42 to 35 mAh/g after five cycles, as depicted in Fig. 6.

The charge-discharge profile in Fig. 6 was measured at potential ranges of 0.001–2.5 V. At a relatively low charge/discharge rate (0.1 C), the specific discharge capacity is larger than that of charge. The discharge process is responsible for sodium-ion intercalation into the graphene interlayer.

At a higher rate, the time during charge and discharge is insufficient to completely intercalate/de-intercalate the sodium ion, resulting in partial sodiation and desodiation of mesocarbon. As a charge/discharge rate increases to 0.5 C, the charge-discharge capacity decreases to 10 mAh/g.

4   Conclusion

The observation of mesocarbon behavior as an anode for SIBs has been performed by analyzing electrochemical results. The studied mesocarbon has a graphene interlayer spacing (d_{002}) of 0.334 nm. Nevertheless, it could still facilitate sodium-ion intercalating at a cathodic peak voltage of 0.001 V and de-intercalating at an anodic peak voltage of 0.12 V. The first three cycles of the CV curve exhibit a stable and reversible intercalation/de-intercalation. The mesocarbon kinetic is dominantly controlled by diffusion processes. After charge-discharge cycling, the resistance increased because of the formation of SEI film on the mesocarbon surface. Subsequently, the specific discharge capacity delivers as high as 42 mAh/g at a scan rate of 0.1 C. The specific discharge capacity decreases as the scan-rate increases.

References

1. Dong, S., Nie, P., Zhang, Flexible Sodium Ion Batteries, in: Flexible Energy Conversion and Storage Devices, edited by C. Zhi and L. Dai (Wiley-VCHVerlag GmbH& Co. KGaA, 2018), pp. 97–123 (2018).
2. Cui, J., Yao, S., Kim, J. K.: Recent progress in rational design of anode materials for high-performance Na-ion batteries, Energy Storage Materials A, 7, pp. 64-114 (2017).
3. Li, F., Wei, Z., Manthiram, A., Feng, Y., Ma, J., Mai, L.: Sodium-based batteries: from critical materials to battery systems, Journal of Materials Chemistry, 7(16), pp.9406-9431 (2019).
4. Morris, J.: Rising Lithium Prices Could Stop The EV Revolution – Or Could They?, Sustainability (2022).
5. Hwang, J. Y., Myung, S. T., Sun, Y. K.: Sodium-ion batteries: Present and future, Chemical Society Reviews, 46(12), 3529-3614 (2017).
6. Luo, W., Schardt, J., Bommier, C., Wang, B., Razink, J., Simonsen, J., Ji, X.: Carbon nanofibers derived from cellulose nanofibers as a long-life anode material for rechargeable sodium-ion batteries, Journal of Materials Chemistry A , 1, pp.10662-10666 (2013).
7. Huang, Y., Zheng, Y., Li, X., Adams, F., Luo, W., Huang, Y., Hu, L.: Electrode Materials of Sodium-Ion Batteries Batteries toward Practical Application, ACS Energy Letters, 3, pp.1604-1612 (2018).
8. Xu, G. L., Amine, R., Abouimrane, A., Che, H., Dahbi, M., Ma, Z. F., Saadoune, I.: Challenges in Developing Electrodes, Electrolytes, and Diagnostics Tools to Understand and Advance Sodium-Ion Batteries, J. Alami, W. L. Mattis, F. Pan, Z. Chen, and K. Amine, Advanced Energy Materials, 8, pp.1-63 (2018).
9. Han, P., Han, X., Yao, J., Yue, L., Zhao, J., Zhou, X., Cui, G.: Mesocarbon microbead based dual-carbon batteries towards low cost energy storage devices, Journal of Power Sources, 393, pp.145-151 (2018).
10. Yan, B. , Wang, G.: Mechanisms and characteristics of mesocarbon microbeads prepared by co-carbonization of coal tar pitch and direct coal liquefaction residue, International Journal of Coal Science and Technology, 6, pp.633-642 (2019).
11. Sun, N., Guan, Z., Liu, Y., Cao, Y., Zhu, Q., Liu, H., Wang, Z., Zhang, P., Xu, B.: Extended "Adsorption – Insertion" Model : A New Insight into the Sodium Storage Mechanism of Hard Carbons, Advanced Energy Materials, 9(32), 1–14, pp. 1–14 (2019).
12. Ardizzone, A., Fregonara, G., Trasatti, A.: Inner and Outer Active Surface of RuO_2 Electrodes, Electrochemica Acta 35, pp. 263–267 (1990).
13. Mathis, T. S., Kurra, N., Wang, X., Pinto, D., Simon, P., Gogotsi, Y.: Energy Storage Data Reporting in Perspective—Guidelines for Interpreting the Performance of Electrochemical Energy Storage System, Advanced Energy Materials, 9, pp.1–13 (2019).
14. Kumar, H., Detsi, E., Abraham, D. P., Shenoy, V. B.: Fundamental Mechanisms of Solvent Decomposition Involved in Solid-Electrolyte Interphase Formation in Sodium Ion Batteries, Chemistry of Materials, 28(24), pp.8930–8941 (2016).